Title	Plasmon enhanced fluorescence studies from aligned gold nanorod arrays modified with SiO2 spacer layers
Authors(s)	Damm, Signe; Fedele, Stefano; Murphy, Antony; Barry, James N.; Dowling, Denis P.; Rice, James H.; et al.
Publication date	2015-05
Publication information	Applied Physics Letters, 106 (18):
Publisher	AIP Publishing
Item record/more information	http://hdl.handle.net/10197/8320
Publisher's statement	The following article appeared in Applied Physics Letters, 106(18) and may be found at http://link.aip.org/link/doi/10.1063/1.4919968. The article may be downloaded for personal use only. Any other use requires prior permission of the author and the American Institute of Physics.
Publisher's version (DOI)	10.1063/1.4919968

Plasmon enhanced fluorescence studies from aligned gold nanorod arrays modified with SiO_2 spacer layers

Signe Damm [1], Stefano Fedele [1], Antony Murphy [2], Kristina Holsgrove [2], Miryam Arredondo [2], Robert Pollard [2], James N. Barry [3], Denis P. Dowling [3], James H. Rice *,[1]

[1] NanoPhotonics Research Group, University College Dublin, Belfield, Dublin 4, Ireland.
[2] Centre for Nanostructured Media, The Queen's University of Belfast, Belfast BT7 1NN, UK
[3] School of Mechanical and Materials Engineering, University College Dublin, Belfield, Dublin 4, Ireland
* Corresponding author. E-mail: james.rice@ucd.ie

Abstract

Here we demonstrate that quasi self-standing Au nanorod arrays prepared with plasma polymerisation deposited SiO_2 dielectric spacers support surface enhanced fluorescence (SEF) while maintaining high signal reproducibility. We show that it is possible to find a balance between enhanced radiative and non-radiative decay rates at which the fluorescent intensity is maximized. The SEF signal optimised with a 30 nm spacer layer thickness, showed a 3.5-fold enhancement with a signal variance of <15% thereby keeping the integrity of the nanorod array. We also demonstrate the decreased importance of obtaining resonance conditions when LSPR is positioned within the spectral region of Au interband transitions. Procedures for further increasing the SEF enhancement factor are also discussed.

Paper

Nanoscale structures made from noble metals such as gold or silver possess localized surface plasmon (LSP) excitations when the structure interacts with light of the correct frequency and polarization [1-2]. When LSPs are formed, strongly enhanced electromagnetic near-fields are generated at the surface of the supporting nanostructure. This property has attracted considerable research interest due to its potential applications in areas such as sensors for medical diagnostics. Sensor technology based on surface enhanced fluorescence enables the detection of a range of different (bio)chemical molecules applicable for medical diagnostics [2]. For medical applications increased signal strength, thereby increased sensitivity and a high degree of signal reproducibility from the plasmon active substrate are important factors. Plasmon active arrays possessing regularly positioned plasmon active sites provide a geometry design that supports a homogenous signal enhancement across a large sample surface area. Modern nanofabrication methodologies enable the creation of a number of different nanostructures with precisely controlled shapes, sizes, and spacing [3-10]. This has extended to the creation of a range of different metallic nanostructures array designs that produce localized surface plasmon resonances (LSPRs) [8-15]. One such design is based on arrays of quasi self-standing metal nanorods [13-15]. Whereby metal nanorods are prepared in a host matrix which when removed produces an array of self-standing nanorods. The design of such arrays enables choice over precise particle shape, length, width and inter-particle coupling thereby controlling the plasmonic properties [13-15].

The presence of LSPRs on plasmonic metal nanostructures can enhance the fluorescence signal from locally situated fluorophores, a process known as surface enhanced fluorescence (SEF) [16-18]. A fluorophore in the vicinity of a metal nanostructure which supports LSPRs can experience both enhancements of non-radiative and radiative decay rates [19-25]. The interaction is threefold involving excitation enhancement, emission enhancement and quenching of the fluorescence emission [20]. The LSPRs contribution to the modification of fluorescence excitation and emission process originates from enhanced local E-fields interacting with the fluorophore. In metal nanostructures the LSPR can be damped and decay through non-radiative and radiative decay channels. The radiative decay channel contributes to the enhanced field while the non-radiative decay channel corresponds to energy lost through thermal dissipation. Whether radiative or non-radiative is the dominant decay process for LSPR damping depends on the metal, the size of the structure and on the excitation wavelength [25]. Above photon energies 1.85 eV for gold, interband transition can occur which introduces an additional decay channel and strongly dampens the plasmon oscillations thereby reducing the possibility for fluorescent (and Raman) enhancement [1, 25]. When the fluorophore is in direct or very close the metal surface the near field of the LSPR and the emitter interact. As a consequence energy from the fluorophore can be absorbed by an electron in the metal which undergoes an intraband transition [24, 25]. Essentially this occurs when the near field of the fluorophore and the nanostructure overlap, this caused an induction of surface charge oscillations in the metal whereby almost all energy is transferred from the fluorophore to the metal and lost through thermal dissipation [25]. This mechanism has shown to be the dominate decay channel at distances below 5 nm and it results in the emission intensity from the fluorophore to be greatly reduced [19-25].

Studies of SiO_2 dielectric coating of plasmon active (fractal) thin gold or silver metal layers have been reported [26-29]. These studies demonstrated that using thin coating (e.g. d=5 nm) SEF can be produced. SiO_2 dielectric spacers have been applied to solution processed randomly organised Au nanorods as a spacer layer [26]. The fluorescence emission from the probe was optimized by modifying the thickness of silica coated gold nanorods. The maximum SEF intensity was obtained at a thickness of d=15 nm [26]. Reineck et al. reported that by using 13 nm Au nanoparticles (Au NPs) they observed strong quenching of the fluorescence intensity when the dye and nanostructure absorption spectra overlapped. They showed that 95% of the fluorescence intensity was quenched up with dye Au NP separation < d=10 nm while only 50% of the fluorescence was quenched when using a different dye where the dye and nanostructure absorption spectra did not overlap [30]. Takahashi et al. also observed the fluorescence intensity being predominantly quenched at low separations of dye and metal nanostructure. For 15 nm Au NPs they observed maximum SEF at a SiO_2 thickness of d=21nm, and by using lifetime measurements it was confirmed that the enhancement was due to coupling to the electromagnetic field created by the excitation of the LSPR [31]. Ge et al. used 30 nm Au NPs and observed maximum SEF at d=40nm. By using COMSOL they determined that the electromagnetic field extended up to d=90nm [32].

Quasi self-standing metallic nanorod arrays possessing a fixed nanorod diameter and inter-rod separation have been widely applied for SERS [12]. A limited number of studies have demonstrated that such nanomaterials can be applied to SEF [33]. Here we demonstrate that such substrates following the removal of the aluminium matrix can support SEF via the use of plasma polymerisation deposited SiO_2. Here we show that SiO_2 enables an optimum layer thickness and does not damage the fragile self-standing nanorod array preserving the plasmonic properties. Plasmon active Au substrate based SEF can be significantly affected by

electronic interband transitions from the valence band to the Fermi level in Au [1, 25]. The presence of interband transitions can lead to nonradiative plasmon damping. Many biological sensing applications require wavelengths to be monitored which are within the interband region. This has motivated our study of SEF from flourophores with optical absorption and emission wavelengths within the interband transition of Au. We demonstrate that effective SEF with excellent signal reproducibility (i.e. signal variance of <15% per 500 μm^2) can be achieved using SiO_2 coated nanorod arrays within this region.

A schematic illustration of the sample i.e. a quasi-ordered free-standing Au nanorod arrays is shown in Fig 1(a). The schematic shows that the array possesses a 70 nm inter rod distance, a rod diameter 35 nm and rod height of 200 nm. The preparation of the Au nanorod arrays are described elsewhere [27]. In brief, the sample was made on a glass substrate base. On this a thin film multilayer was prepared by magnetron sputtering, consisting of 8 nm tantalum pentoxide (Ta_2O_5), 5 nm gold and a 300 nm aluminium film. Porous alumina (PAO) templates were formed by anodization of the aluminium in 0.3 M sulphuric acid (~1 °C) at constant voltage using a platinum counter-electrode. Au nanorods were then grown in the PAO template by electrodeposition on the conducting 5 nm thick Au underlayer. We have found that the substrates produce better Raman and fluorescence signal if annealed before depositing the fluorophore. The substrates were annealed at 200 degrees C for 2 hours left to cool and then etched for 30 min. in 30 mM NaOH to remove the PAO template the Au nanorods were buried in. The plasma polymerisation deposition was performed using the OpenAir® atmospheric plasma jet system combined with the PlasmaPlus® liquid precursor delivery unit manufactured by PlasmaTreat GmbH (Steinhagen, Germany). The silicon dioxide coatings were deposited using the liquid precursor Tetraethyl-orthosilicate (TEOS, Sigma-Aldrich), which is characteristically used in the semiconductor industry for applying SiO_2 layers. The plasma jet head was mounted onto a 3-axis precision gantry which enables the movement of the plasma at a nozzle to substrate height of 18mm over the substrates. The depositions were performed in a raster pattern at a traverse speed of 75 mm/sec and 4 mm raster step gap. The thickness of the SiO_2 was determined by using a light profilometer. The fluorophore used was Rhodamine 6G (R6G). As a reference sample, we produced a glass slide with a 30 nm SiO_2 film coverage. R6G was added to the samples by drop-deposition. Each sample (500 μm^2) was deposited with 10 µL of 10^{-6} M R6G and left to dry. Raman and fluorescence spectra were recorded using a custom-built, open-bench Raman system in epi-fluorescence backscattering configuration with 532 nm and 473 nm excitation. Fluorescence imaging and lifetime measurements were also done using an epi-fluorescence setup using a pulsed laser [8-10]. The surface topography was measured using Atomic force microscopy (AFM) in contact mode at a scan rate of 12 mm/sec.

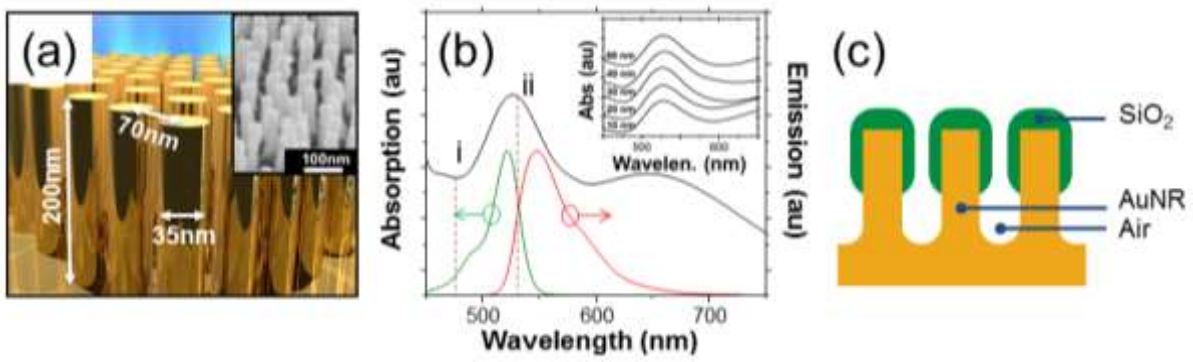

Fig. 1 (a) Schematic drawing of the Au nanorod array, inset is shown an SEM of the nanorod array. (b) Normal incidence optical absorption spectrum of nanorod array (black) with emission (red) and absorption spectrum (green) of probe molecule R6G. Marked i and ii are the wavelength position for excitation radiation at 473 and 532 nm respectively. Insert shows the absorption spectra for samples with d=10-50 nm SiO_2 (c) Schematic of the sample preparation for the distance dependent SEF study.

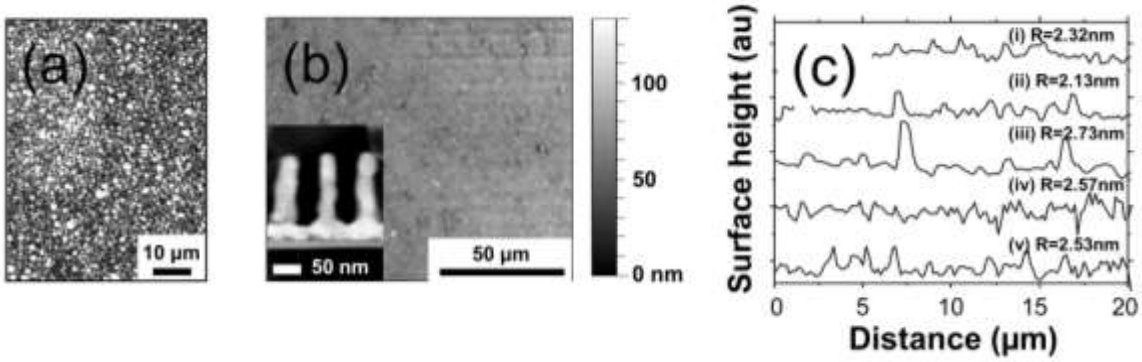

Fig. 2. (a) SEM image and (b) AFM image of a sample with 30 nm SiO_2 spacer layer. Insert shows a cross-sectional TEM image. (c) AFM line profiles measured for different thicknesses of SiO_2 spacer layer depositions (i) 10, (ii) 20, (iii) 30, (iv) 40 and (v) 50 nm. The mean square roughness (R) parameters are also shown.

Optical absorption and fluorescence spectra of the fluorophore were recorded, along with the optical absorption spectrum of the Au nanorod array. The results are shown in Fig 1(b). Absorption spectra of the arrays were measured at normal incidence using a UV-visible spectrometer before adding the fluorophore. The absorption spectrum for the substrate shows a broad peak with maxima at c.a. 530 nm which overlaps with the absorption and fluorescence bands of the R6G fluorophore. To study the distance dependent SEF from R6G on Au nanorod arrays we used SiO_2 as dielectric spacer layer. SiO_2 is known to be chemically inert, optically transparent and stable which are beneficial for distance dependent SEF studies [30, 34]. Absorption spectra from the samples were recorded (shown as inset in Fig. 1(b)). The absorption spectra show no change with increasing SiO_2 deposition indicating that the surface plasmon resonance wavelength is independent of spacer layer thickness. The schematic shown in Fig. 1(c) shows the sample morphology after SiO_2 deposition. We expect the tips of the nanorods to be primarily coated.

Fig. 2 (a-c) show the surface morphology after SiO_2 deposition. Fig. 2(a) shows an SEM image of an Au nanorod sample with 30 nm SiO_2 deposition. Fig. 2(b) show an AFM image of the same sample. The images show that the surface consists of large sphere shaped particulates of SiO_2. Studies have shown that sputtering SiO_2 films at 30 nm produces similar microscopy surface image features with the surface roughness been reported to be less than 1 nm [28]. Fig. 2 (b)-insert shows a cross-sectional TEM image. The image shows the presence of up-right nanorods and SiO_2 layer. XRD data of the sample shows that as you progress deeper into the sample from the top of the SiO_2 into areas between the nanorods, silicon can be detected though at progressively lower concentration. Fig. 2(c) shows line profiles extracted from the AFM images for SiO_2 thicknesses d=10-50 nm. As can be seen from the

line profiles, the roughness parameter is similar for different thicknesses of SiO_2. The square mean roughness (R) calculated from these line profiles is $R_{average}$ = 2.5 nm.

The fluorescence and Raman spectra were recorded simultaneously. The fluorescence spectrum is measured as a broad peak at c.a. 550 nm with Raman bands superimposed onto the fluorescence spectrum. Fig. 3(a) shows the Raman spectra obtained at different thicknesses of SiO_2. No Raman bands were observed from the dye recorded on glass with SiO_2 demonstrating that the observed Raman bands are plasmon assisted i.e. surface enhanced Raman scattering (SERS). We observed a strong SERS signal when there was no SiO_2 present between Au and R6G. As SiO_2 was introduced the SERS response vanished. In parallel, the fluorescence emission intensity on glass was compared to that from the Au nanorod array, see Fig. 3(b). The fluorescence intensity from the fluorophore adsorbed directly on the Au nanorod array was reduced (see graph "0 nm" and "glass"). The reason for the decrease in fluorescence intensity is due to the direct contact between fluorophore and metal, causing the florescence emission to be predominantly deactivated through metal-induced energy transfer. Fig. 3(b) also shows the change fluorescence intensity when adding SiO_2 dielectric spacer layers between Au nanorods and the fluorophore, showing that the fluorescence signal is distance dependent. The intensity of the fluorescence signal was monitored as a factor of spacer layer thickness d=10-50 nm on the Au nanorod array. The fluorescence signal is seen to increase above that for glass with increasing spacer thickness. At d=30 nm spacer thickness the fluorescence signal is seen to maximise, thereafter declining with increasing SiO_2 spacer thickness.

We also studied the distance dependent SEF using 473 nm excitation wavelength (see Fig. 3(d)). The enhancement factor (EF) vs. thickness was plotted. EF is calculated as $EF = I_{Au\ NR} / I_{Glass}$ where $I_{Au\ NR}$ is the intensity measured from the Au nanorod array and I_{Glass} is the fluorescence intensity measured from the glass slide with SiO_2. The plot shows a maximum EF of > 3 at d=30 nm. We observed a similar trend in EF even though the spectral position of the LSPR of the Au nanorod array does not overlap with the wavelength of the excitation laser. Previous studies have shown that for SiO_2 thicknesses above d=10 nm, the choice of excitation wavelength has a minor effect on the resulting signal intensity [30]. But below d=10 nm the electromagnetic field strength is highly depend on whether or not the wavelength is in resonance with the localized surface plasmon. Even below 10 nm we do not observe a major difference in EF for 473 and 532 nm excitation wavelengths. The explanation for the similarities in EF for both wavelengths is that we are probing within the interband transition region of Au [1, 25, 35-36]. Probing with a larger excitation wavelength would minimize the energy losses which are at a minimum around 650 nm. Furthermore it would also be optimal to have the LSPR, dye absorption and emission bands spectrally positioned outside the interband transition region to fully take advantage of resonant excitation.

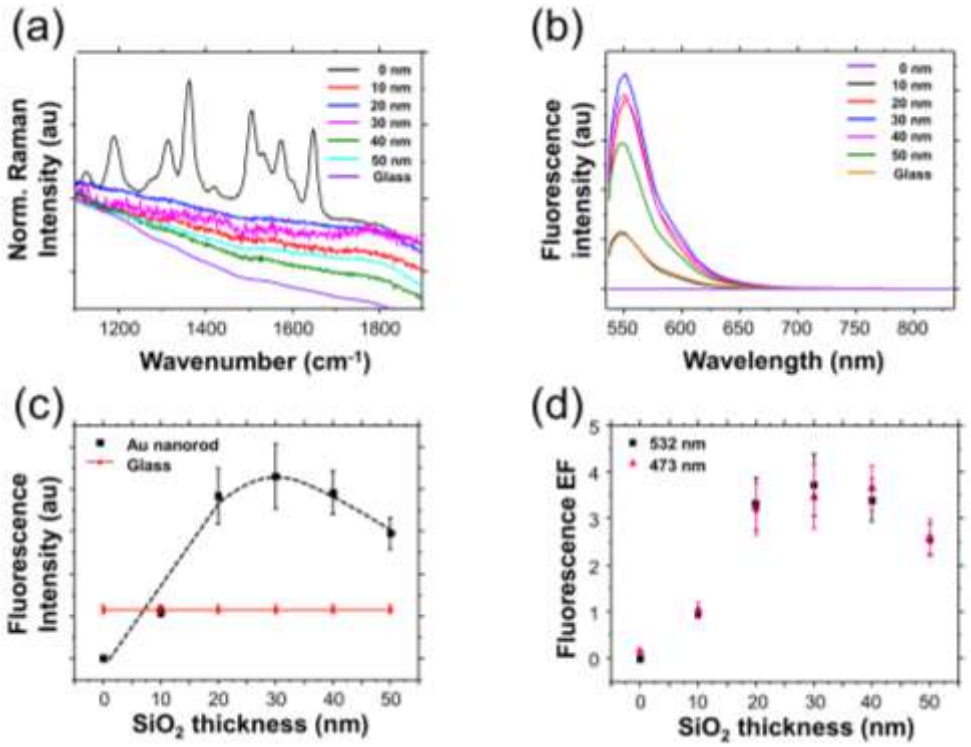

Fig. 3. (a) Distance dependent SERS from R6G on Au nanorod array. For reference a plot of the signal obtained from glass with 30nm SiO_2 spacer layer is also shown. (b) A plot of fluorescence intensity from R6G on Au nanorod array and glass substrates with varying SiO_2 spacer layer thicknesses. Recorded using λ_{ex} = 532 nm. (c) Distance dependent SEF from R6G on Au nanorod array ■ and glass with SiO_2 ●. (d) A plot of the distance dependent SEF enhancement factor recorded for different excitation wavelengths (λ_{ex} = 532 nm ■, λ_{ex} = 473 nm ▲).

The observed distance dependent enhancement of the fluorescence intensity indicates that the fluorescence signal is plasmonically enhanced by the Au nanorods and that the quenching by the metal is dramatically reduced by the introduction of a spacer layer. To support this theory we measured the average lifetimes from each sample. There exists a competition between the non-radiative (k_{nr}) rate and radiative (Γ_{rad}) rate of the fluorescence intensity. The presence of the metallic nanostructure causes an increase in radiative and non-radiative decay pathways available. The lifetime of the fluorophore in its excited state (τ) is inverse proportional to both decay rates as expressed by $\tau = 1/ \Gamma_{rad} + k_{nr}$ where k_{nr} and Γ_{rad} correspond to non-radiative and radiative decay rates. Quenching of the fluorescence emission is dominant at short distances between metal and fluorophore. The non-radiative rate decays rapidly with distance (d^{-3}) whereas the enhancement of the radiative rate is long range effect and therefore by using an appropriate spacer layer to separate the fluorophore from the metal it is possible to increase and maximize the emission intensity [20]. We want to decrease the non-radiative rate and minimize the decrease in radiative rate. The non-radiative rate, radiative rate and excitation rate have been shown to all decrease with distance to the metal surface [19-25, 37, 38]. Note that modifications to the radiative rate extend to much larger distances than the non-radiative rate. We therefore expect that directly on the "bare" Au both rates are maximized and we observe the lowest lifetime. We observed a decreased fluorescence lifetime for the fluorophore on the Au nanorod arrays compared to glass (Fig 4(a)). When a

spacer layer was added the lifetime increased. On spacer layers of 10 and 20 nm the fluorophore had a longer lifetime (3.20 ± 0.06 and 3.57 ± 0.05 ns respectively) than when situated on 'bare' Au nanorod arrays (2.62 ± 0.12 ns). It is noted that this value is relatively long lived which we assign to the probe molecule been drop deposited creating areas of probe molecule agglomerates. When the spacer layer thickness increased to d=30-50 nm the lifetime was further increased (3.96 ± 0.21, 4.11 ± 0.11 and 4.08 ± 0.23 ns respectively). The distance dependent change in lifetime is shown in Fig. 4(b). The lifetime values have been normalized with respect to the lifetime measured from R6G on glass with SiO_2. By increasing the spacer layer between fluorophore and metal the decay rates decrease. But the decrease in non-radiative decay rate happens more rapidly compared to the decrease in radiative rate. We are therefore able to observe SEF at spacer thickness d=30 nm. This decrease in both rates leads to a total increase in lifetime. This is in line with established theory [19-25, 37, 38]. It is seen that even at 50 nm SiO_2 spacer layer the fluorophore is still plasmonically affected by the Au nanorod arrays, since the lifetime has not fully recovered. The fluorescent lifetime of the fluorophore on glass is 4.69 ± 0.18 ns.

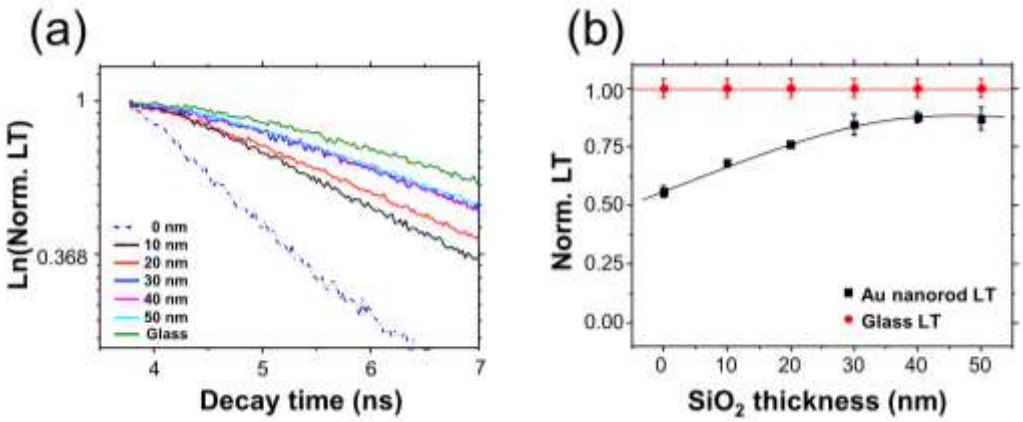

Fig. 4 (a) Fluorescence lifetime decay plots from Au nanorods with different SiO_2 thicknesses and from glass with 30 nm SiO_2 deposition. (b) Normalised distance dependent lifetimes from Au nanorods ■ and glass ● .

We have demonstrated that it is possible to achieve SEF using Au nanorod arrays prepared with plasma polymerisation deposited SiO_2 dielectric spacers. In correlation with fluorescence lifetime measurements we have shown that the fluorophore was affected by the plasmonic field at the surface of the Au nanorods and that it was possible to effectively reduce quenching and produce SEF using the right SiO_2 spacer thickness. The fluorescent lifetime was seen to increase with increasing SiO_2 spacer layer thickness since E-field and the metal-induced energy transfer decreased with distance from the Au nanorod surface. SERS signal intensity from R6G was seen to reduce dramatically as the SiO_2 spacer layer thickness increased. The SEF signal was maximised when using a 30 nm spacer layer thickness resulting in a 3.5-fold enhancement within the interband transition region of the Au nanorods. We observed no different in EF when changing the excitation laser from 532 nm to 473 nm, due to dampening by interband transitions in Au. SiO_2 was shown to form a film with moderate topography when creating the spacer layer on Au nanorod arrays. This provided an environment for reproducible SEF signal enhancement. The average variation in signal intensity across the entire sample area was maintained at < 15% per 500 μm^2 owing to the

small surface roughness of SiO_2 and the homogeneity of the Au nanorod arrays. Improvements in the methodology of sample preparation ex. probe and SiO_2 deposition methodology potentially may improve the reproducibility factor further.

The Nanophotonics and Nanoscopy Research Group is supported by Science Foundation Ireland SFI grants 11/RFP.1/MTR/3151, 12/IP/1556 and 09/RFP/PHY2398. The Centre for Nanostructured Media acknowledges the Engineering and Physical Sciences Research Council (EPSRC - UK) for financial support (Grants EP/H000917, EP/I014004).

References

1. S. Hayashi, T. Okamoto. Plasmonics: visit the past to know the future. Journal of Physics D: Applied Physics. **45**, 433001 (2012).

2. M.I. Stockman. Optics Express, **19**, 22029-22106 (2011)

3. N. Al-Attar, I. Kopf, E. Kennedy K. Flavin, S. Giordani, J.H. Rice. Chem. Phys. Lett., **535**, 146-151 (2012)

4. F. Lordan, S. Damm, E. Kennedy, C. Mallon, R.J. Forster, T.E. Keyes, J.H. Rice. Plasmonics **8**, 1567-1575 (2013)

5. E. Kennedy, R. Al-Majmaie, M. Al-Rubeai, D. Zerulla, J.H. Rice. RSC Advances **3**, 13789-13795 (2013)

6. R.W. Martin, P.R. Edwards, R.A. Taylor, J.H. Rice, J.H. Na, J.W. Robinson, J.D. Smith, C. Liu, I.M. Watson. J. Physica Status Solidi (a) **202**, 372-376 (2005)

7. J.H. Rice, R. A. Oliver, J.W. Robinson, J.D. Smith, R.A. Taylor, G.A.D. Briggs, M.J. Kappers, C.J. Humphreys, S. Yasin. Physica E, **21**, 546-550 (2004).

8. F. Lordan, J.H. Rice, B. Jose, R.J. Forster, T.E. Keyes. J. Phys. Chem. C, **116**, 1784–1788 (2012)

9. S. Damm, N.C. Carville, B.J. Rodriguez, M. Manzo, K. Gallo, J.H. Rice. J. Phys. Chem. C., **116**, 26543-26550 (2012)

10. S. Damm, N.C. Carville, M. Manzo, K. Gallo, S.G. Lopez, T.E. Keyes, R.J. Forster, B.J. Rodriguez, J.H. Rice. Appl. Phys. Lett. **103**, 083105(2013)

11. A. Murphy, Y. Sonnefraud, A. V. Krasavin, P. Ginzburg, F. Morgan, J. McPhillips, G. Wurtz, S. A. Maier, A. V. Zayats, R. Pollard. Appl. Phys. Lett. **102**, 103103 (2013).

12. M.D. Doherty, A. Murphy, R.J. Pollard, P. Dawson. Phys. Rev. X. **3**, 011001 (2013).

13. G.A. Wurtz, R.J. Pollard, W. Hendren, G.P. Wiederrecht, D.J. Gosztola, V.A. Podolski, A.V. Zayats. Nat. Nanotech. **6**, 106-110 (2011).

14. P.R. Evans, R. Kullock, W.R. Hendren, R. Atkinson, R.J. Pollard, L.M. Eng. Advan. Funct. Mat., **18**, 1075-1079 (2008).

15. D.P. Lyvers, J.M. Moon, A.V. Kildishev, V.M. Shalaev, A. Wei. ACS nano. **2**, 2569-2576 (2008).

16. S.Y. Liu, L. Huang, J.F. Li, C. Wang , Q. Li, H.X. Xu, H.L Guo, Z.M. Meng , Z. Shi, Z.Y Li. J. Phys. Chem. C., **117**, 10636-10642 (2013).

17. E. Fort, S. Grésillon. J. Phys. D: Appl. Phys., **41**, 013001 (2008).

18. A.M. Gabudean, M. Focsan, S. Astilean. J. Phys. Chem. C., **116**, 12240-12249 (2012).

19. R. Carminati, J. J. Greffet, C. Henkel, J. M. Vigoureux, J. M. Optics Communications, 261(2), 368-375 (2006).

20. J. Azoulay, A. Débarre, A. Richard, P. Tchénio, P. EPL (Europhysics Letters), 51(4), 374 (2000).

21. M. Thomas, J.J. Greffet, R. Carminati, J.R. Arias-Gonzalez, Applied physics letters, 85(17), 3863-3865 (2004).

22. P. Bharadwaj, B. Deutsch, L. Novotny, Optical antennas. Advances in Optics and Photonics, 1(3), 438-483 (2009).

23. V. V. Klimov, M. Ducloy, V. S. Letokhov, Quantum Electronics, 31(7), 569-586 (2001).

24. F. Hubenthal, Plasmonics, 8(3), 1341-1349 (2013).

25. N. A, Issa, R. Guckenberger, R. Optics express, **15**(19), 12131-12144 (2007).

26. M. Muniz-Miranda. J. Raman Spec. **35**, 839-842 (2004).

27. P.J. Tarcha, J. DeSaja-Gonzalez, S. Rodriguez-Llorente. Appl. Spec., **53**, 43-48 (1999).

28. W.B. Lacy, J.M. Williams, L.A. Wenzler, T.P. Beebe, J.M. Harris. Anal. Chem., **68**, 1003-1011 (1996).

29. V.I. Kukushkin, A.B. Vankov, I.V. Kukushkin. JETP letters, 342-347 (2013).

30. P. Reineck, D. Gómez, S. H. Ng, M. Karg, T. Bell, P. Mulvaney, U. Bach, ACS nano, **7**, 6636-6648 (2013).

31. T. Takahashi, A. Kudo, S. Kuwabata, A. Ishikawa, A. Ishihara, Y. Tsuboi, T. Torimoto. J. Phys. Chem. C., **117**, 2511-2520 (2012).

32. W. Ge, X.R. Zhang, M. Liu, Z. Lei, R.J. Knize, Y. Lu. Theranostics, **3**, 282 (2013).

33. S. Damm, F. Lordan, A. Murphy, M. McMillen, R. Pollard, J.H. Rice. Plasmonics, **9**, 1371-1376 (2014).

34. N. Yin, Y. Liu, L. Liu, J. Lei. T.T. Jiang, H.J. Wang, L.X. Zhu, X.L. Xu. J. Alloy Compounds, **581**, 6-10 (2013).

35. L.B. Scaffardi, J.O. Tocho. Nanotechnology, **17**, 1309–1315 (2006).

36. P.R. West, S. Ishii, G.V. Naik. N.K. Emani, V.M. Shalaev. A. Boltasseva. Laser, Photon. Rev. **4**, 795-808 (2010).

37. A. Campion, A.R. Gallo, C.B. Harris, H.J. Robota, P.M. Whitmore. Chem. Phys. Lett., **73**, 447-450 (1980).

38. C.D. Geddes, J.R. Lakowicz. J. Fluor., **12**, 121-129 (2002).